JOURNAL OF GEOPHYSICAL RESEARCH: SPACE PHYSICS, VOL. 118, 1351–1365, doi:10.1002/jgra.50107, 2013

Proton thermal energetics in the solar wind: Helios reloaded

Petr Hellinger,[1,2] Pavel M. Trávníček,[3,1] Štěpán Štverák,[1,2] Lorenzo Matteini,[4,5] and Marco Velli[4,6]

Received 10 August 2012; revised 28 December 2012; accepted 31 December 2012; published 9 April 2013.

[1] The proton thermal energetics in the slow solar wind between 0.3 and 1 AU is reinvestigated using the Helios 1 and 2 data, complementing a similar analysis for the fast solar wind [Hellinger et al., 2011]. The results for slow and fast solar winds are compared and discussed in the context of previous results. Protons need to be heated in the perpendicular direction with respect to the ambient magnetic field from 0.3 to 1 AU. In the parallel direction, protons need to be cooled at 0.3 AU, with a cooling rate comparable to the corresponding perpendicular heating rate; between 0.3 and 1 AU, the required cooling rate decreases until a transition to heating occurs: by 1 AU the protons require parallel heating, with a heating rate comparable to that required to sustain the perpendicular temperature. The heating/cooling rates (per unit volume) in the fast and slow solar winds are proportional to the ratio between the proton kinetic energy and the expansion time. On average, the protons need to be heated and the necessary heating rates are comparable to the energy cascade rate of the magnetohydrodynamic turbulence estimated from the stationary Kolmogorov-Yaglom law at 1 AU; however, in the expanding solar wind, the stationarity assumption for this law is questionable. The turbulent energy cascade may explain the average proton energetics (although the stationarity assumption needs to be justified) but the parallel cooling is likely related to microinstabilities connected with the structure of the proton velocity distribution function. This is supported by linear analysis based on observed data and by results of numerical simulations.

Citation: Hellinger, P., P. M. Trávníček, Š. Štverák, L. Matteini, and M. Velli (2013), Proton thermal energetics in the solar wind: Helios reloaded, *J. Geophys. Res. Space Physics*, *118*, 1351–1365, doi:10.1002/jgra.50107.

1. Introduction

[2] The proton thermal energetics in the solar wind is far from being understood. In situ observations indicate that protons need to be heated from the inner to the outer heliosphere. The necessary proton heating is usually calculated from the isotropic fluid approximation neglecting heat fluxes and assuming a stationary flow $\boldsymbol{u}=\boldsymbol{u}(R)$ (for symbol definitions, see Appendix B) as follows:

$$nk_B\boldsymbol{u}\cdot\nabla T = -\frac{2}{3}nk_BT\nabla\cdot\boldsymbol{u} + Q \tag{1}$$

where Q is the average heating rate (note that the total heating rate is usually defined as 3/2 Q). For a radially expanding solar wind with a constant radial velocity v_{sw} and assuming that the temperature depends on the radial distance R as $T\propto R^{\xi}$, it is easy to derive the necessary heating rate [cf., *Verma et al.*, 1995; *Vasquez et al.*, 2007]

$$Q = \left(\frac{4}{3}+\xi\right)\frac{nk_BTv_{sw}}{R}. \tag{2}$$

[3] As the proton temperature typically decreases quite slower than $\propto R^{-4/3}$, the necessary heating rate is often comparable to nk_BTv_{sw}/R.

[4] In the weakly collisional solar wind, protons exhibit important temperature anisotropies [*Marsch et al.*, 1982b; *Hellinger et al.*, 2006] and the isotropic fluid approximation is questionable [cf., *Matteini et al.*, 2012]. It is generally necessary to treat the parallel and perpendicular temperatures separately. In this case, the expressions for the parallel and perpendicular heating rates are more complicated [*Marsch and Richter*, 1987] and depend on the orientation of the magnetic field. Contribution of the heat fluxes and collisions to the proton thermal energetics are typically negligible, and without an external energy source, the proton parallel and perpendicular temperatures would vary following the double adiabatic (CGL) prediction [*Chew et al.*, 1956]. However, in situ observations

[1]Astronomical Institute, AS CR, Prague, Czech Republic.
[2]Institute of Atmospheric Physics, AS CR, Prague, Czech Republic.
[3]Space Sciences Laboratory, University of California, Berkeley, California, USA.
[4]Dipartimento di Fisica e Astronomia, Università degli Studi di Firenze, Florence, Italy.
[5]Imperial College, London, UK.
[6]Jet Propulsion Laboratory, California Institute of Technology, Pasadena, California, USA.

Corresponding author: P. Hellinger, Astronomical Institute, AS CR, Bocni II/1401, Prague 14100, Czech Republic (Petr.Hellinger@asu.cas.cz)

2169-9380/13/10.1002/jgra.50107

show strong deviations from CGL, with the perpendicular proton temperature decreasing with distance slower than expected while the parallel proton temperature decreases faster than predicted close to the sun and slower than expected further away. *Hellinger et al.* [2011] (referred hereafter as Paper 1) used Helios 1 and 2 data to quantify the proton heating rates in the fast solar wind. Paper 1 found that closer to the sun ($R \lesssim 0.6$ AU), protons need to be cooled in the parallel direction and heated in the perpendicular direction (and/or there needs to be an energy transfer from the parallel to perpendicular direction), and these cooling and heating factors have the same order of magnitude, around 0.3 AU. Further away from the sun ($R \gtrsim 0.6$ AU), there is a need of parallel and perpendicular heating, and these heating rates are of the same order, at around 1 AU. On average, the protons need to be heated with heating rates comparable to those obtained from the isotropic fluid approximation, equation (2). Paper 1 also suggests that the interaction between slow and fast streams leads to an overall deceleration of the fast streams [cf., *Arya and Freeman*, 1991], which contributes to the proton thermal energetics [cf., *Miyake et al.*, 1988].

[5] A natural energy source for the proton heating is the strong wave activity/turbulence. High-frequency quasi-parallel Alfvén ion cyclotron waves heat ions efficiently in the perpendicular direction through the cyclotron resonance [*Hollweg and Isenberg*, 2002]. These waves may originate at the sun and propagate in the expanding solar wind with a continuously decreasing ion cyclotron frequencies until they become resonant with and become damped by ions [*Schwartz et al.*, 1981; *Tu and Marsch*, 2001]. This mechanism heats preferentially minor ions, and it is questionable whether there is enough energy in the quasi-parallel ion cyclotron waves to account for the observed proton energization [*Schwartz et al.*, 1981; *Hellinger et al.*, 2005]. The usual suspect for the proton-energization mechanism in the solar wind is the dissipation of the magnetohydrodynamic (MHD) turbulence [*Matthaeus and Velli*, 2011]; however, the MHD turbulence and its energetics in the expanding solar wind are not well understood [cf., *Grappin and Velli*, 1996; *Matthaeus et al.*, 1999], the fluctuating magnetic energy decreases with a rate which is comparable to the theoretical (WKB) prediction for noninteracting Alfvén waves. The dissipation of MHD turbulence is understood even less: it is not clear how the MHD cascade proceeds at small, kinetic scales; the applicability of the weak-turbulence approximation in the dissipation region is questionable; and the role of coherent intermittent structures in the dissipation is not understood [*Carbone*, 2012; *Osman et al.*, 2012]. Consequently, the heating rates, i.e., the energy repartition on different species and in different directions (parallel and perpendicular with respect to the ambient magnetic field) due to the energy cascade of the MHD turbulence, are also largely unknown. The best estimates of the turbulence cascade/dissipation rate are based on the third-order stationary Kolmogorov-Yaglom law [*Politano and Pouquet*, 1998; *Carbone et al.*, 2009] in the inertial (dissipationless) frequency range. These estimates [*MacBride et al.*, 2008; *Osman et al.*, 2011] indicate that there is typically enough energy in the turbulent cascade to heat protons. However, in high cross-helicity flows, energy cascade rates estimated from the stationary Kolmogorov-Yaglom law may become much weaker [*Smith et al.*, 2009].

[6] Which processes are responsible for the proton parallel cooling close to the sun is another open question. The interaction of protons with high-frequency Alfvén ion cyclotron wave leads only to a weak parallel cooling [*Hollweg and Isenberg*, 2002]. MHD turbulence may lead to a pitch angle scattering, which may cause an energy transfer from the parallel to perpendicular direction. In this case, there is, however, a question as to why the parallel proton cooling takes place only close to the sun, since by 1 AU, protons are heated in both the parallel and perpendicular directions with similar heating rates. To better constrain the processes responsible for the proton thermal energetics, it is necessary to look at the microstructure of the proton velocity distribution function and its radial evolution. The proton velocity distribution function typically exhibits two populations, a denser core and a secondary/beam population drifting with respect to the core (along the ambient magnetic field in the antisunward direction). The proton beam-core differential velocity decreases with the distance following the local Alfvén velocity [*Marsch et al.*, 1982b]. This differential velocity importantly contributes to the total (effective) proton parallel temperature and to the observed parallel cooling. A linear Vlasov-Maxwell theory predicts multiple instabilities, which may result in such a core-beam proton system [*Daughton and Gary*, 1998], and Helios observations indicate their presence [*Marsch and Livi*, 1987; *Tu et al.*, 2004]. Signatures of these instabilities are also found in the Ulysses data [*Goldstein et al.*, 2000; *Matteini et al.*, 2013]. These instabilities decelerate the beam population with respect to the core, and this energy is transferred to waves and to the particle heating. Beam instabilities may naturally explain the proton parallel cooling. Indeed, the numerical simulation of the proton beam-core system in the expanding solar wind clearly shows an efficient parallel cooling and perpendicular heating [*Hellinger and Trávníček*, 2011] in qualitative agreement with Helios observations.

[7] In this paper, we estimate the parallel and perpendicular heating/cooling rates in the slow solar wind in the inner heliosphere using in situ Helios 1 and 2 data complementing the work of Paper 1. We discuss these results in the context of previous theoretical, observational, and simulation results. The paper is organized as follows: In section 2, we analyze the slow solar wind and estimate the heating/cooling rates assuming a constant radial velocity as well as an accelerating solar wind. In section 3, the present results are compared with the previous observations, properties and roles of Coulomb collisions and heat fluxes are considered, the radial evolution of the proton distribution function is discussed, and the obtained heating/cooling rates are compared with the estimated turbulent dissipation rates at 1 AU and with results of kinetic simulations. Finally, the results are summarized in section 4.

2. Helios Observations

[8] Here we use data from ion analyzers and fluxgate magnetometers onboard the Helios 1 and 2 spacecraft [*Marsch et al.*, 1982a; *Marsch et al.*, 1982b]. The Helios 1 data are from the period 1974–1985 whereas Helios 2 data are from 1976–1980; these observations include a transition between the solar minimum and maximum. The Helios analyzers

employ a quadrispherical ion electrostatic deflector that analyzes ions with respect to their charge-per-energy ratio. A full three-dimensional spectrum, 32 channels (exponentially distributed between 155 V and 15.3 kV) times 9×16 angular channels (with the resolution $5^\circ \times 5^\circ$ making use of the spacecraft rotation), is measured every 40.5 s. In this paper, we use these 3-D energy spectra to calculate the basic moments of the proton velocity distribution function; the contribution of alpha particles is removed by using their different charge-to-mass ratio [*Marsch et al.*, 1982b]. We calculate the proton number density, n, radial component of the mean velocity, v_R, parallel and perpendicular temperatures, $T_\parallel$ and $T_\perp$, and both nonzero components of the heat flux tensor, $q_\parallel$ and $q_\perp$. Note that the temperatures and heat fluxes are calculated for the whole observed proton distribution functions. A secondary proton population which is ubiquitous in the solar wind contributes to the parallel temperature and to the heat fluxes.

2.1. Radial Dependencies

[9] Here we try to determine the radial dependence of the parallel and perpendicular temperatures in the slow solar wind in order to estimate the proton energetics and necessary heating/cooling rates. We use the whole data set of 3-D ion energy spectra from both Helios spacecrafts but select only those data where it was easy to separate alpha particles from protons. Here we only investigate the slow solar wind. Therefore, we have selected only those cases in which the proton radial velocity is $v_R < 400$ km/s.

[10] These data are shown in Figure 1, where points represent the observed proton radial velocity v_R (top), magnitude of the magnetic field B (middle), and proton density n as a function of the radial distance R (bottom). The top panel of Figure 1 clearly reveals the speed cut-off at 400 km/s. The radial dependence of the proton number density and the magnitude of the magnetic field could be fitted using the least-square nonlinear regression for the power law dependence $y = ax^\xi$ as

$$B \simeq 5.7(R/R_0)^{-1.6} n\mathrm{T} \text{ and } n \simeq 11(R/R_0)^{-1.9} \mathrm{cm}^{-3}, \qquad (3)$$

respectively, where $R_0 = 1$ AU. The solid curves on Figure 1 (middle and bottom) show the fitted dependencies according to equation (3).

[11] Results for the proton temperatures calculated from the 3-D energy spectra are shown in Figure 2; here, points represent combined Helios 1 and 2 observations, with (top) parallel proton temperature $T_\parallel$, (middle) perpendicular proton temperature $T_\perp$, (bottom) average proton temperature T given as functions of the radial distance R. All the temperatures decrease with R. These dependencies may be approximated by the fits

$$\begin{aligned} T_\parallel &\simeq 8.1 \cdot 10^4 (R/R_0)^{-0.59} K, \\ T_\perp &\simeq 5.2 \cdot 10^4 (R/R_0)^{-0.58} K, \\ T &\simeq 6.2 \cdot 10^4 (R/R_0)^{-0.58} K, \end{aligned} \qquad (4)$$

which are overplotted in Figure 2.

[12] Finally, we calculate heat fluxes from the 3-D energy spectra. Figure 3 shows points, obtained from the combined Helios 1 and 2 observations, denoting (top) heat flux $q_\parallel$, (middle) heat flux $q_\perp$, and (bottom) average heat flux q as functions of the radial distance R. Heat fluxes are given in

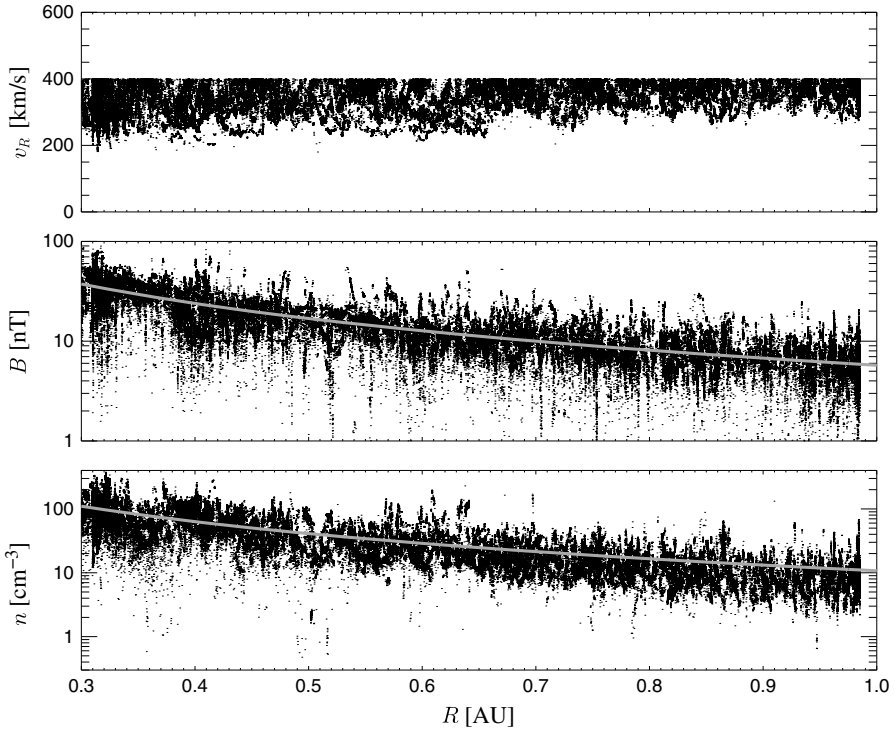

Figure 1. Helios 1 and 2 observations: Points show (top) proton radial velocity v_R, (middle) magnitude of the magnetic field B, and (bottom) proton density n as a function of the radial distance R. Overplotted gray solid curves show the fitted results (see the text).

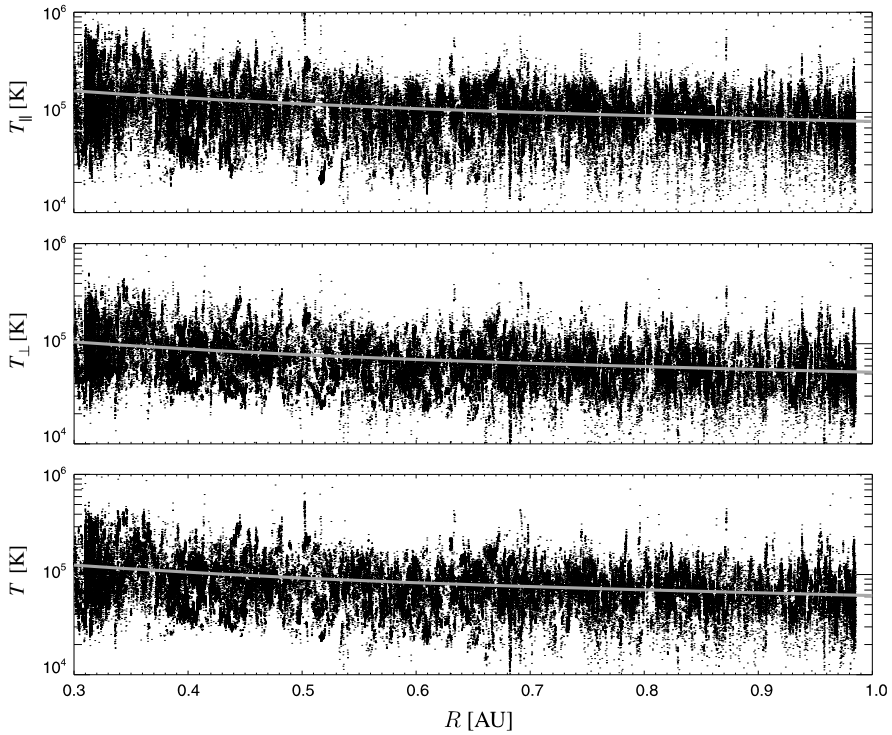

Figure 2. Helios 1 and 2 observations: Points show (top) parallel proton temperature $T_\parallel$, (middle) perpendicular proton temperature $T_\perp$, and (bottom) average proton temperature T as functions of the radial distance R. Overplotted gray solid curves show fitted results (see the text).

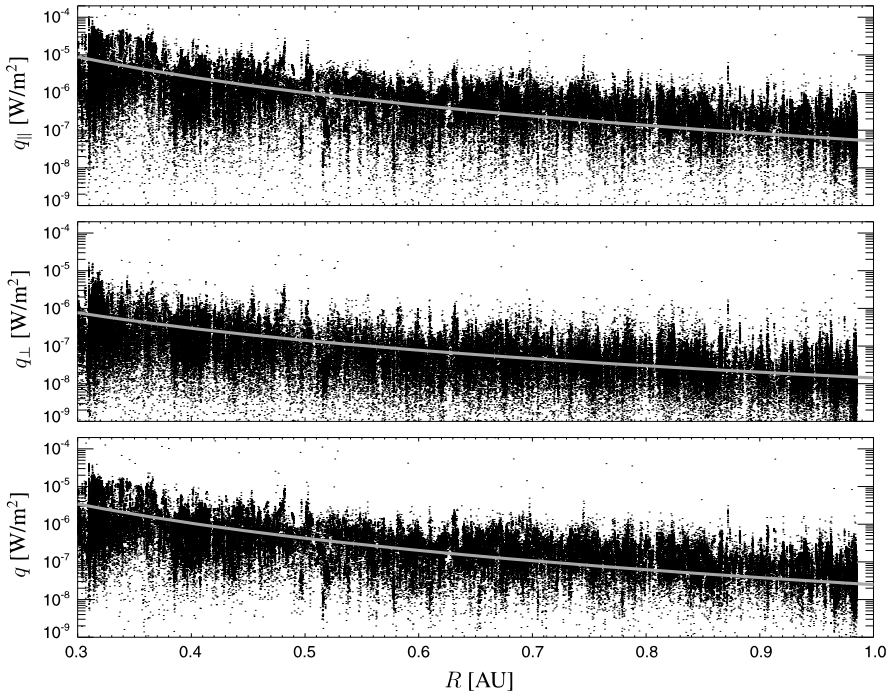

Figure 3. Helios 1 and 2 observations: Points show (top) heat flux $q_\parallel$, (middle) heat flux $q_\perp$, and (bottom) average heat flux q as functions of the radial distance R. Overplotted gray solid curves show fitted results (see the text).

units of W/m ^{2} = 1000 erg/s/cm^2. The overplotted gray solid curves show the fitted results:

$$\begin{aligned} q_{\parallel} &\simeq 5.2 \cdot 10^{-8} (R/R_0)^{-4.3} \mathrm{W/m^2}, \\ q_{\perp} &\simeq 1.4 \cdot 10^{-8} (R/R_0)^{-3.3} \mathrm{W/m^2}, \\ q &\simeq 2.5 \cdot 10^{-8} (R/R_0)^{-4.1} \mathrm{W/m^2}. \end{aligned} \tag{5}$$

[13] From the nonlinear regression, we estimated the relative variances for the base values and power indices for the densities and temperatures of a few percentage points. For the heat fluxes, the estimated error is slightly bigger.

2.2. Heating Rates

[14] The fitted results from the previous section can be now used to test the proton thermal energetics. The heating rates, $Q_{\parallel}$ and $Q_{\perp}$, are given as (assuming a stationary solar wind flow $\partial u/\partial t = 0$)

$$\begin{aligned} Q_{\parallel} &= n k_B \left[\boldsymbol{u} \cdot \nabla T_{\parallel} + 2 T_{\parallel} \nabla_{\parallel} \cdot \boldsymbol{u} - 2 \nu_T \left(T_{\perp} - T_{\parallel} \right) \right] \\ &\quad + \nabla \cdot \left(q_{\parallel} \boldsymbol{b} \right) - 2 q_{\perp} \nabla \cdot \boldsymbol{b}, \\ Q_{\perp} &= n k_B \left[\boldsymbol{u} \cdot \nabla T_{\perp} + T_{\perp} \nabla_{\perp} \cdot \boldsymbol{u} + \nu_T \left(T_{\perp} - T_{\parallel} \right) \right] \\ &\quad + \nabla \cdot \left(q_{\perp} \boldsymbol{b} \right) + q_{\perp} \nabla \cdot \boldsymbol{b}, \end{aligned} \tag{6}$$

where $\nabla_{\parallel} = \boldsymbol{b}(\boldsymbol{b} \cdot \nabla)$ and $\nabla_{\perp} = \nabla - \nabla_{\parallel}$ and ν_T is the collisional isotropization frequency (see Appendix B).

[15] For the calculation of $Q_{\parallel}$ and $Q_{\perp}$, we assume here a model with a constant radial velocity $v_{sw} = 350$ km/s, and for the proton density, we assume $n = 11 (R/R_0)^{-2} \mathrm{cm}^{-3}$, which is close to the observed values and compatible with a constant radial velocity. The temperatures and heat fluxes are assumed to follow the fitted results, equations (4) and (5), while the magnetic field is assumed to follow the Parker spiral (with the radial and transverse components of the magnetic field, $B_r \propto \cos\theta (R/R_0)^{-2}$ and $B_t \propto \sin\theta (R/R_0)^{-1}$, with $\theta = 45°$). Figure 4 shows the resulting values $|Q_{\parallel}|$, $Q_{\perp}$, as well as the average heating rate $Q = (Q_{\parallel} + 2Q_{\perp})/3$ as functions of the radial distance. In the top panel, the solid curve shows positive values of $Q_{\parallel}$ whereas the dotted curve shows negative values of $Q_{\parallel}$.

[16] Figure 4 shows that protons need to be heated in the perpendicular direction. The model predicts a parallel cooling around 0.3 AU with an absolute value comparable with perpendicular heating rate. The parallel cooling slowly disappears, and at around 1 AU, the protons need to be heated in both the parallel and perpendicular directions with similar heating rates. In a region with weak cooling rates, the contribution of Coulomb collisions and heat fluxes to the anisotropic energy budget is small but nonnegligible (in the vicinity of the point where the parallel heating rate is zero, the contribution of Coulomb collisions and heat fluxes is of course important, but this is a singular situation).

[17] For the average heating rate Q, we get the following results for the constant velocity solar wind model:

$$Q \simeq 1.5 \cdot 10^{-17} (R/R_0)^{-3.2} \mathrm{W/m^3}. \tag{7}$$

[18] From the error analysis for the fitted results for the proton density and temperatures, we estimate the relative variances for the base value and the power index for the average heating rate Q to be about 10–20%.

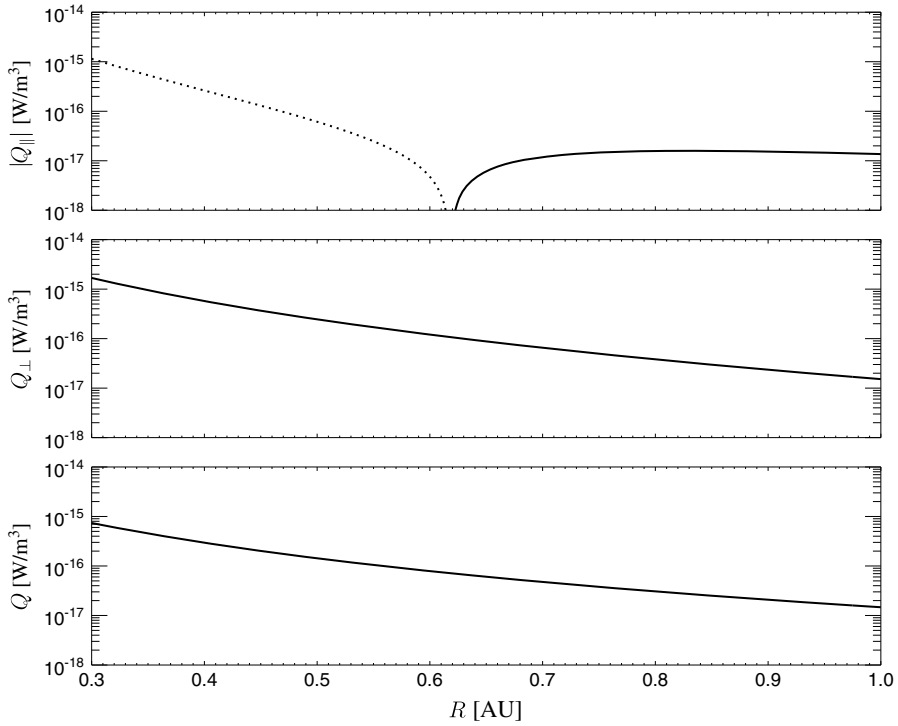

Figure 4. Estimated heating rates from the fitted data: (top) absolute value of the parallel heating rate $Q_{\parallel}$ (the dotted and solid lines denote negative and positive values of $Q_{\parallel}$, respectively), (middle) perpendicular heating rate $Q_{\perp}$, and (bottom) average heating rate Q.

[19] For further analysis of the data, it is useful to express the heating rates in terms of a ratio between the proton energy $E_p = nk_BT$ and the expansion time $t_E = R/v_{sw}$

$$Q_E = \frac{E_p}{t_E} = \frac{nk_BTv_{sw}}{R}. \quad (8)$$

[20] This rate also naturally appears in equation (2). Figure 5 summarizes the heating rates obtained here for the slow solar wind and the heating rates of Paper 1 for the fast solar wind (assuming a constant velocity) in terms of Q_E. It shows the estimated heating rates from the fitted data: the top panel shows the parallel heating rates, the middle panel shows the perpendicular heating rates, and the bottom panel shows the average heating rates, all normalized to Q_E. The solid lines show the results for the slow solar wind whereas the dashed lines show the corresponding results obtained in the fast solar wind [*Hellinger et al*., 2011].

[21] Figure 5 shows that the heating and cooling rates are typically a nonnegligible fraction of Q_E and the results in the fast and slow solar wind have comparable magnitudes in terms of Q_E (as well as in terms of the heating/cooling rates per unit volume). Figure 5 also indicates that the parallel and perpendicular heating rates may be relatively well approximated by the linear relations

$$\frac{Q_\parallel}{Q_E} \sim -0.75 + 1.2\frac{R}{R_0} \text{ and } \frac{Q_\perp}{Q_E} \sim 0.80 - 0.32\frac{R}{R_0}, \quad (9)$$

respectively. For comparison in the fast solar wind [*Hellinger et al*., 2011], one gets (for the constant velocity model)

$$\frac{Q_\parallel}{Q_E} \sim -0.58 + 0.84\frac{R}{R_0} \text{ and } \frac{Q_\perp}{Q_E} \sim 0.88 - 0.47\frac{R}{R_0}. \quad (10)$$

[22] Finally, the ratio between the average heating rates Q and the expansion rate Q_E is relatively constant between 0.3 and 1 AU; in the slow solar wind, one gets

$$\frac{Q}{Q_E} \sim 0.28 + 0.18\frac{R}{R_0} \quad (11)$$

whereas in the fast solar wind, one gets (for the constant velocity model)

$$\frac{Q}{Q_E} \sim 0.39 - 0.031\frac{R}{R_0}. \quad (12)$$

3. Discussion

3.1. Comparison With Previous Observational Results

[23] In this paper, we used the least-square nonlinear regression for the power law dependence $y = ax^\xi$ whereas in Paper 1, we used the least-square linear regression for log $y = a + \xi \log x$. The latter model is not generally correct, as it alters the error distribution and consequently violates the basic assumptions for the regression. We have, however, checked that the nonlinear regression and the linear logarithmic regression give almost the same results for the fast solar wind investigated in Paper 1. For the slow solar wind, this is no longer true and the least-square nonlinear regression

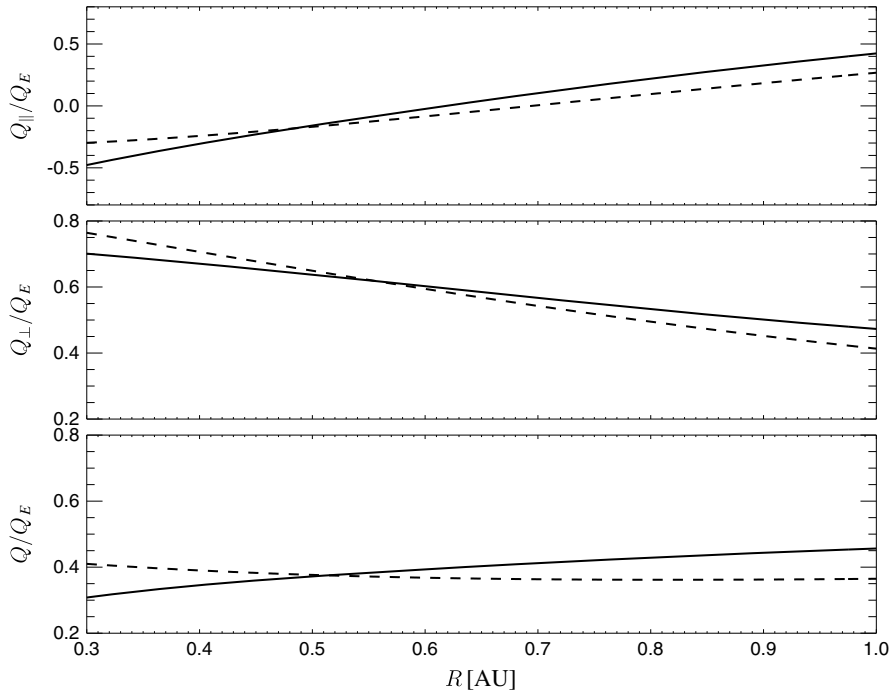

Figure 5. Estimated heating rates from the fitted data: (top) parallel heating rate $Q_\parallel$, (middle) perpendicular heating rate $Q_\perp$, and (bottom) average heating rate Q normalized to the expansion rate Q_E based on the dimensional analysis (equation 8). For comparison, the dashed lines show the corresponding results obtained (for the constant-velocity model) in the fast solar wind [*Hellinger et al*., 2011].

should be used. It is interesting to note that compared to the fast solar wind, the slow solar wind streams are more variable, which is possibly due to their different origins.

[24] The fitted dependences of the parallel and perpendicular temperatures in the fast solar wind (see Paper 1) are in good agreement with the results of *Marsch et al*. [1982b]. However, in the case of the slow solar wind (here we use $v_{sw} < 400\,\mathrm{km/s}^{-1}$), we have a weaker radial decrease of the two temperatures with respect to those reported by *Marsch et al*. [1982b] for 300 km/s $< v_{sw} <$ 400 km/s even including estimated errors (here we have estimated the relative variance for the power indices to be a few percentage points; *Marsch et al*., [1982b] estimated the relative variance to be 10–20%). One possible explanation of this discrepancy is that we include velocities below 300 km/s as there are indications of the overall acceleration of the slow solar wind streams (see Figure 1 and note missing points in figures 18 and 19 in the work of *Marsch et al*. [1982b] for v_{sw} 200–300 km/s above $R \gtrsim 0.6$). In order to test this hypothesis, we have separated the Helios data to subsets with velocities in the ranges 200–300, 300–400, 400–500, 500–600, 600–700, and 700–800 km/s following *Marsch et al*. [1982b]. For these subsets, we have fitted the proton number density and the parallel and perpendicular temperatures as $a(R/R_0)^{\xi}$. The results of this fitting procedure are given in Table 1, where we added the results of the corresponding fitting of the parallel and perpendicular temperatures ($\propto (R/R_0)^{\xi_M}$) by *Marsch et al*. [1982b]. The relative variance for the fitted parameters is within a few percentage points for our results.

[25] The fitted results for 300–400 km/s give steeper slopes compared to the case with velocities below 400 km/s, as expected (the proton temperature and the solar wind velocity are well correlated) [cf., *Elliott et al*., 2012]. From Table 1, it follows that while the radial gradients estimated by *Marsch et al*. [1982b] are generally steeper than what we observe, these results are roughly consistent when including the estimated errors. Furthermore, *Marsch et al*. [1982b] analyzed data from the solar minimum, whereas here, we included also data from the solar maximum.

[26] Table 1 also shows that the proton number density decreases almost as fast as R^{-2} in slower solar wind streams, whereas for faster streams, it decreases slower than R^{-2}. The latter results are in agreement with the expected consequence of the interaction between fast and slow solar wind streams, but there are no clear indications of the faster-than-R^{-2} decrease of the density, which would be consistent with the apparent acceleration/increase of the minimum velocity with the distance. This is likely a consequence of the inclusion of many slow solar streams with different properties.

Table 1. Results of the Fitting of the Radial Profiles of the Proton Number Density, $n = n_0(R/R_0)^{\xi_n}$ (Where $R_0 = 1$ AU), and of the Proton Parallel and Perpendicular Temperatures, $T_{\|} = T_{\|0}(R/R_0)^{\xi_{\|}}$ and $T_{\perp} = T_{\perp 0}(R/R_0)^{\xi_{\perp}}$ for Different Solar Wind Velocity Ranges. $\xi_{\|M}$ and $\xi_{\|M}$ are the Corresponding Results of the Similar Fitting $T_{\|,\perp} \propto (R/R_0)^{\xi_{\|,\perp M}}$ by *Marsch et al*. [1982b]

	Velocity Range (km/s)					
	200–300	300–400	400–500	500–600	600–700	700–800
n_0 [cm^{-3}]	14	10	6.1	4.5	3.1	2.7
ξ_n	–1.9	–1.9	–1.9	–1.7	–1.8	–1.8
$T_{\|0}$[*MK*]	0.049	0.081	0.15	0.24	0.29	0.32
$\xi_{\|}$	–0.49	–0.76	–0.70	–0.58	–0.55	–0.56
$\xi_{\|M}$		–1.0	–0.85	–0.80	–0.75	0.69
$T_{\perp 0}$[*MK*]	0.034	0.052	0.10	0.18	0.24	0.27
$\xi_{\perp}$	–0.50	–0.73	–0.79	–0.79	–0.81	–0.92
$\xi_{\perp M}$		–0.90	–0.86	–1.1	–1.1	–1.2

3.2. Model

[27] We estimated the parallel and perpendicular heating (cooling) rates in the stationary constant velocity model assuming the Parker spiral magnetic field with 45° between the radial direction and the ambient magnetic field at 1 AU. The results based on the constant velocity approximation may be modified by the interaction between fast and slow streams. There are indications of an overall acceleration of slow solar wind streams, which is likely due to this effect. We have not analyzed the possible impact of the stream-stream interaction on the proton energetics, as this is a complex phenomenon including compression and rarefaction regions and requires a more detailed study [cf. *Elliott et al*., 2012].

[28] Here (and in Paper 1), we used the Parker spiral magnetic field with 45° at 1 AU. The expected angle, however, depends on the solar wind velocity. For the solar wind velocity 350 km/s assumed here, the expected angle at 1 AU is about 50°. Repeating the calculation with 50°, we get weaker parallel cooling at 0.3 AU by about 10% and stronger parallel heating at 1 AU by 20%, and $Q_{\|}$ crosses zero at 0.53 AU. The perpendicular heating rate $Q_{\|}$ decreases by 5–10%, whereas the average heating rate Q increases by about 5% compared to the predictions for 45°. For larger angles, the difference increases.

[29] Similarly, for the fast solar wind with 700 km/s, the expected angle is about 30°. For this angle (assuming the constant velocity model), the parallel cooling is necessary from 0.3 to 1 AU; $Q_{\|}$ is about $-0.4Q_E$ and increases (in a quadratic-like way) to $-0.1Q_E$. The perpendicular heating rate $Q_{\perp}$ decreases (roughly linearly) from about $0.8Q_E$ at 0.3 AU to about $0.6Q_E$ at 1 AU. The average heating rate remains comparable within a few percentage points to the prediction based on the 45°.

[30] The angle of the Parker spiral at 1 AU is important for the determination of parallel and perpendicular heating rate while its influence on the average heating rate is small. There are, however, large variations of the magnetic field compared to the theoretical Parker spiral [*Borovsky*, 2010] due to, e.g., the MHD turbulence. We expect that the actual values of the parallel and perpendicular heating rates (and, to a lesser extent, the average heating rate) will be influenced by the large-scale magnetic field radial evolution. We expect that our basic results will not be altered, the parallel cooling rates would be an important fraction of Q_E at 0.3, and the perpendicular and average heating rates would be an important fraction of Q_E.

3.3. Role of Coulomb Collisions

[31] The contribution of Coulomb collisions to the proton energetics is negligible in the fast solar wind, which is essentially collisionless. In the more collisional slow solar wind

[*Livi and Marsch*, 1986; *Kasper et al*., 2008], the collisions weakly contribute to the parallel energy budget close to the sun where the magnitude of the parallel cooling/heating rates are weaker than the perpendicular heating rates.

[32] Wind observations at 1 AU by *Kasper et al*. [2008] indicate that the local collisionality (also used as a proxy for the proton collisional age) $\tau = v_T t_E$ (i.e., the ratio between the expansion time t_E and the proton temperature isotropization time $1/v_T$ in the present case) characterizes the solar wind properties in a better way than the solar wind velocity. Here we quickly investigate the properties of the local collisionality τ in the Helios data. Figure 6 shows a frequency of observations in the space (R,τ) in the left panel and in the space (v_{sw},τ) in the right panel. The left panel of Figure 6 suggests that τ is about constant (or slowly decreases) in the solar wind and that in general τ is not a good proxy for the proton collisional age. Indeed, the collisional frequency is basically proportional to $n/T^{3/2} \propto R^{-2-3\xi/2}$ (where we suppose $T \propto R^{\xi}$); the expansion time is proportional to R so that τ is constant or decreases for $\xi \gtrsim -2/3$, which is often satisfied in our fitted results.

[33] The right panel of Figure 6 demonstrates the well-known anticorrelation between the solar wind velocity and the local collisionality. It also shows a larger spread/variability of the local collisionality in the slow solar wind.

3.4. Heat fluxes

[34] In the fast solar wind, the proton heat fluxes are important being comparable to the saturation heat flux $q_{sat} = n(k_B T_{\|})^{3/2}/m^{1/2}$ (see Paper 1), but they do not significantly contribute to the proton thermal energetics (because of the fast solar wind velocities). In the slow solar wind, the parallel heat flux $q_{\|}$ weakly contributes to the parallel energy budget close to the sun where the magnitude of the parallel cooling/heating rates are weaker than the perpendicular heating rates. It is therefore interesting to look at the (typically more important) parallel heat flux in the solar wind. Figure 7 shows a frequency of Helios observations in the space $(R, q_{\|}/q_{sat})$ in the left panel and in the space $(v_{sw}, q_{\|}/q_{sat})$ in the right panel. The left panel of Figure 7 indicates that the ratio between the parallel and saturation heat fluxes remains about constant or slowly decreases with the radial distance. The right panel of Figure 7 shows that the parallel heat flux (with respect to the saturation one) is more important in the fast solar wind than in the slow solar wind and that there is a large variability of the ratio $q_{\|}/q_{sat}$ in slower solar wind streams.

3.5. Microstructure

[35] The observed important proton temperature anisotropies and heat fluxes result from complicated proton velocity distribution functions [*Marsch*, 2012]. The left panel of Figure 8 shows an example of a 2-D cut (isocontours) of the observed 3-D velocity distribution function measured by Helios 2 at 0.3 AU (1976, day 111, 04:45:24). Figure 8 (left panel) shows that the proton velocity distribution function has (at least) two components. The more abundant (termed here *core*) exhibit a temperature anisotropy $T_{\perp} > T_{\|}$, whereas the second less abundant, field-align population (termed here *beam*) has rather the opposite anisotropy; this beam temperature anisotropy is, however, difficult to discern as the two populations overlap. The presence of the beam importantly contributes to the total proton temperature anisotropy and to the proton heat flux. In this paper (and in Paper 1), we have only used few moments to describe the proton velocity distribution. One way how to improve the description is to fit the distribution function by a model one. A useful model which is typically used is a superposition of two bi-Maxwellian populations drifting with respect to each other along the ambient magnetic field [*Goldstein et al*., 2010]. Here we use a simpler model; the core is assumed to be bi-Maxwellian, whereas the beam is fitted as an isotropic Maxwellian population. Right panel of Figure 8 shows a result of such a fitting procedure. The fitted

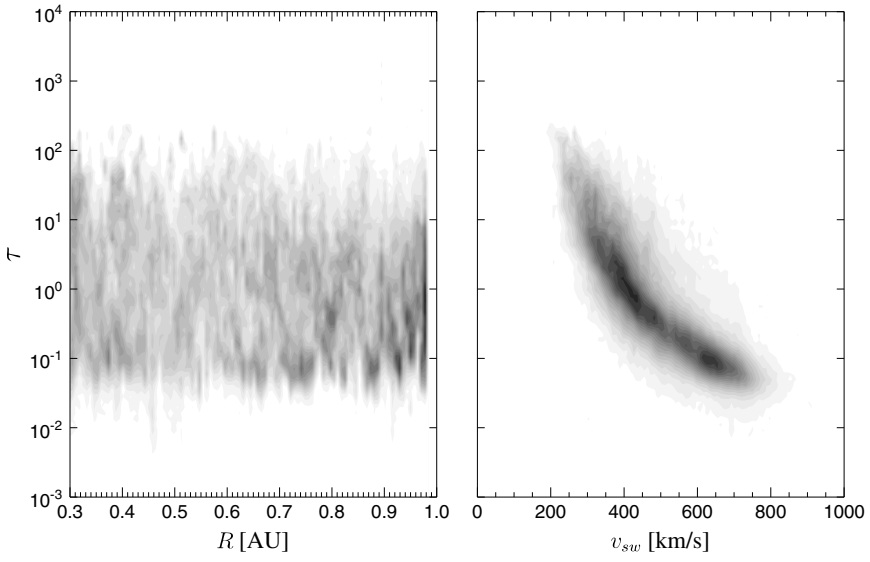

Figure 6. Local collisionality versus the radial distance and the solar wind velocity: color scale plots of the frequency of Helios observations in the plane (R,τ) in the left panel and in the plane (v_{sw},τ) in the right panel. Black corresponds to maximum values and white to minimum ones.

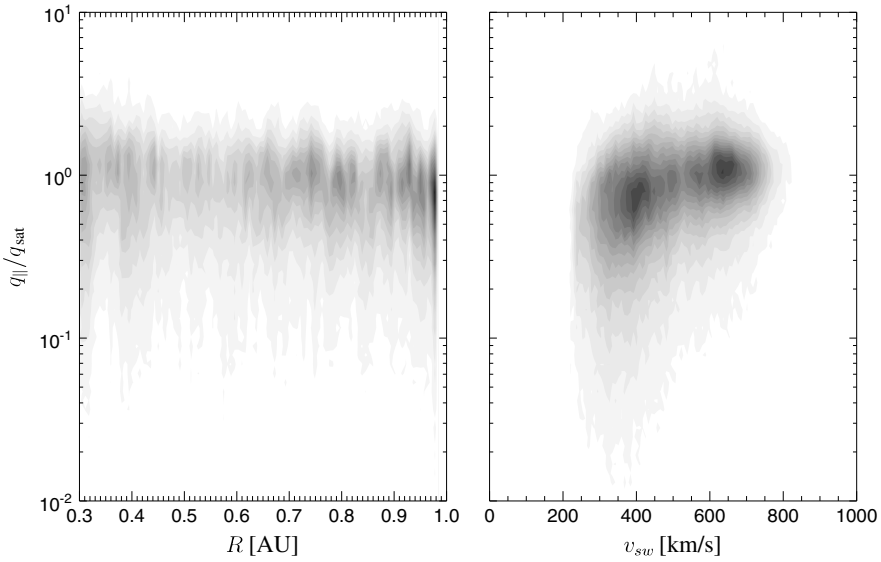

Figure 7. Parallel proton heat flux versus the solar wind velocity and the local collisionality: frequency of Helios observations in the plane $(R, q_{\parallel}/q_{sat})$ in the left panel and in the plane $(v_{sw}, q_{\parallel}/q_{sat})$ in the right panel. Black corresponds to maximum values and white to minimum ones.

results reproduce the observations relatively well in this case, but one cannot expect that this model characterizes all observations for all purposes. The fitting procedure gives, however, some quantitative estimates of the proton beam-core structure and its radial evolution.

[36] Here we report preliminary results of our fitting procedure for the slow solar wind $v_{sw} < 400$ km/s using Helios 1 and 2 data. Figure 9 shows the beam number density n_b (with respect to the total proton density n) as a function of the radial distance on the top panel. The bottom panel displays the relative field-aligned velocity between the beam and core populations v_{bc} as a function of the radial distance. The overplotted solid gray curve shows the average local Alfvén velocity (determined from equation (3)). Figure 9 shows that in the slow solar wind, the fitted beam densities are about 10% and that the beam-core velocity decreases with the distance as the local Alfvén velocity but the fitted data have a very large scatter around these values.

[37] For comparison, we performed a similar analysis in the fast solar wind $v_{sw} > 600$ km/s. Figure 10 shows the relative beam number density n_b/n as a function of the radial distance on the top panel. The bottom panel displays the relative beam-core velocity v_{bc} as a function of the radial distance. Overplotted solid gray curve shows the average local Alfvén velocity (determined from equation (5) of Paper 1). Figure 10 shows that the fitted beam densities are about 4 % and that the beam-core velocity decreases with the distance as the local Alfvén velocity. The fitted data have a

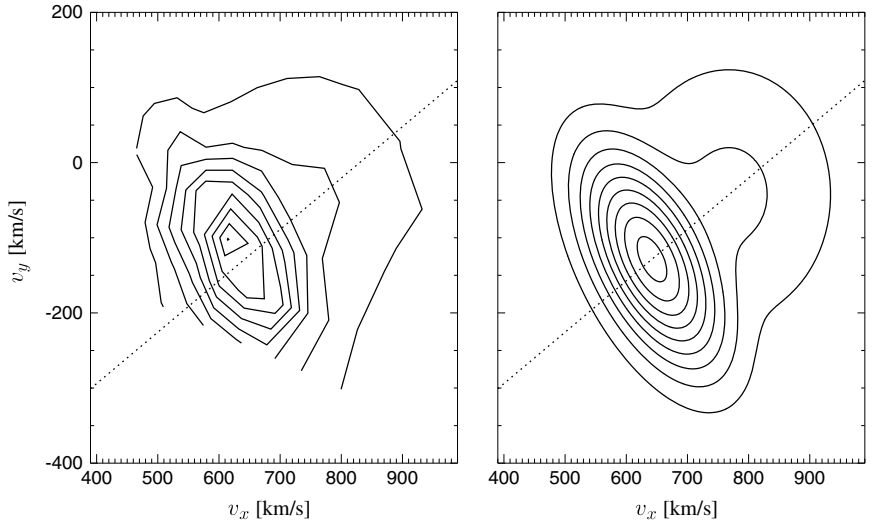

Figure 8. Example of the proton velocity distribution function at 0.3 AU: (left) Isocontours of a 2-D cut of the $f_{\rm p} = f_{\rm p}(v_x, v_y)$ observed by Helios 2 at 0.3 AU. (right) Results of a fitting procedure, isocontours of the fitted velocity distribution function in the same plane. Velocities v_x and v_y are in the GSE coordinates. Dotted lines show the projection of the ambient magnetic field.

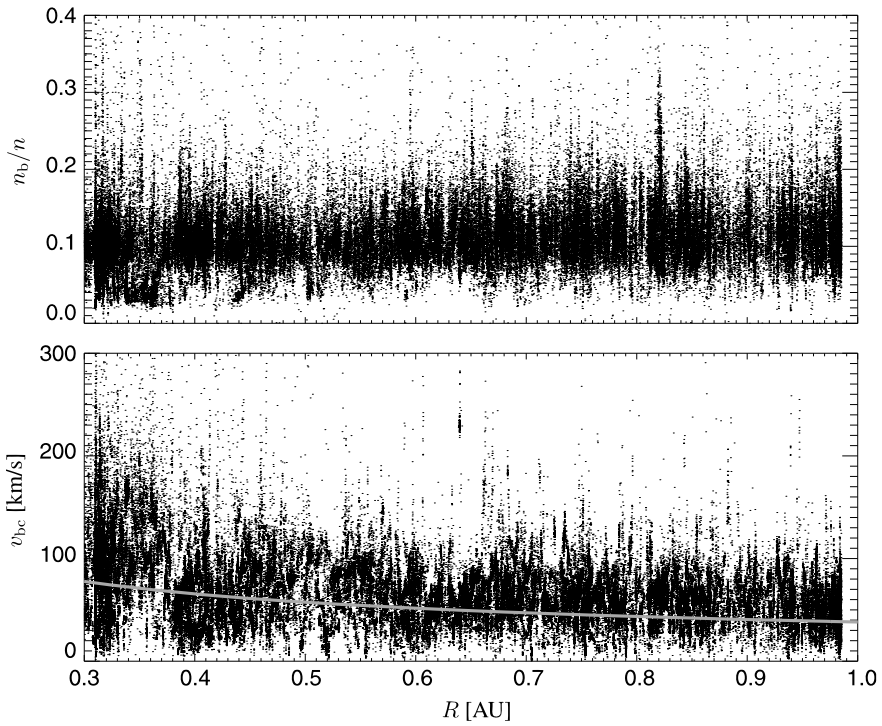

Figure 9. Helios 1 and 2 in the slow solar wind: (top) relative beam number density (with respect to the total proton density) and (bottom) relative field-aligned velocity between the beam and core populations as functions of the radial distance. Overplotted solid gray curve shows the average local Alfvén velocity.

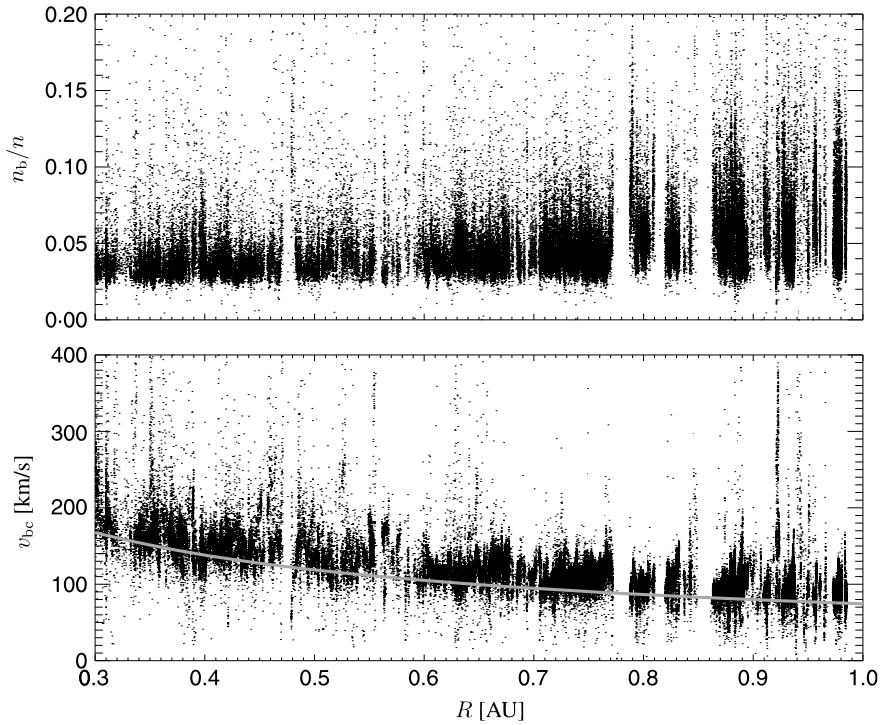

Figure 10. Helios 1 and 2 observations in the fast solar wind: (top) relative beam number density (with respect to the total proton density) and (bottom) relative field-aligned velocity between the beam and core populations as functions of the radial distance. Overplotted solid gray curve shows the average local Alfvén velocity.

large scatter around these values, but the scatter is smaller compared to the slow solar wind.

[38] The fitted beam densities are about half the values estimated by *Marsch et al*. [1982b] (Figure 14) directly from the velocity distribution function. This is not surprising, as the obtained fitted values depend strongly on the used model. Assuming an anisotropic (bi-Maxwellian) beam, we obtain much stronger beam populations (and smaller beam-core relative velocities). The fitted beam-core relative velocities are in good agreement with the results of *Marsch et al*. [1982b] (Figure 12) showing that the relative velocities decrease with the distance following roughly the local Alfvén velocity. This decrease importantly contributes to the proton parallel cooling. The estimated contribution of the relative beam-core velocity to the total proton parallel temperature

$$T_v = \frac{n_b}{n}\frac{m}{k_B}v_{bc}^2 \tag{13}$$

based on the fitted results is comparable to the actual decrease of the total proton parallel temperature in both fast and slow solar winds. The Helios observations indicate that beam-core structure is ubiquitously present in the solar wind from 0.3 AU. The secondary beam population is likely generated closer to the sun, possibly due to ion-acoustic wave activity connected with the parametric instabilities of large-amplitude fluctuations/turbulence [*Araneda et al*., 2008; *Matteini et al*., 2010; *Valentini et al*., 2011] or due to oblique kinetic Alfvén waves [*Li et al*., 2010; *Osmane et al*., 2010] or other effects. These processes typically lead to a parallel heating connected with the formation of the beam, and their relation with the observed parallel cooling is unclear. More detailed analysis of beam-core structure is beyond the scope of this paper and will be subject of future works.

3.6. Turbulent Heating

[39] The average heating rates obtained in this paper in the slow solar wind translate to the heating rates (per unit mass) $\varepsilon_h = 3/2Q/(nm)$

$$\varepsilon_h \simeq 1.3\cdot 10^3 (R/R_0)^{-1.2}\mathrm{W/kg}. \tag{14}$$

[40] The Kolmogorov-Yaglom law in the homogeneous media assuming a stationarity (and other assumptions, cf., *Wan et al*., [2009]) may be given

$$\nabla_{\delta\boldsymbol{x}}\cdot\langle\delta\boldsymbol{z}^{\mp}|\delta\boldsymbol{z}^{\pm}|^2\rangle = -4\varepsilon_t^{\pm} \tag{15}$$

where $\varepsilon_t^{\pm}$ is the pseudoenergy cascade rate of the corresponding Elsässer variables $\boldsymbol{z}^{\pm}$ (see Appendix A). The energy cascade rate is then $\varepsilon_t = \left(\varepsilon_t^{+} + \varepsilon_t^{-}\right)/2$. *MacBride et al*. [2008] used the stationary Kolmogorov-Yaglom law to estimate the turbulent cascade rates in the solar wind at 1 AU using time series from the ACE spacecraft. For the slow solar wind ($v_{sw} < 400$ km/s), they obtained the turbulent cascade rate of about $\varepsilon_t \sim 2\cdot 10^3$W/kg (depending on the model of turbulence used to estimate $\nabla_{\delta\boldsymbol{x}}\cdot\langle\delta\boldsymbol{z}^{\mp}|\delta\boldsymbol{z}^{\pm}|^2\rangle$ and the direction with respect to the magnetic field). *Osman et al*. [2011] used multipoint measurements from Cluster II to estimate the turbulent cascade rate through the stationary Kolmogorov-Yaglom law turbulent energy cascade rate $\varepsilon_t \sim 5\cdot 10^3$W/kg; the typical velocity of the solar wind during their analysis is 400 km/s so that these results are related to the slow solar wind and are comparable with the results of *MacBride et al*. [2008]. The turbulent energy cascade rate seems to be sufficient to heat protons in order to explain the Helios observations in the slow solar wind, although the calculation of the energy cascade rate based on the Kolmogorov-Yaglom law generally requires spatial cross-correlations in three dimensions, but available estimates are typically based on relatively limited data sets [cf., *Osman et al*., 2011].

[41] For the fast solar wind, Paper 1 obtained the heating rates in the case of the constant-velocity model

$$\varepsilon_h \simeq 7.9\cdot 10^3 (R/R_0)^{-1.8}\mathrm{W/kg}. \tag{16}$$

[42] In the fast solar wind, the energy cascade rate seems to exhibit a strong anisotropy with respect to the ambient magnetic field having the cascade rate of the order $\varepsilon_t \sim 10^4$W/kg in the perpendicular direction, whereas in the parallel direction, the cascade rate is of the order of $\varepsilon_t \sim 10^3$W/kg [*MacBride et al*., 2008]. The (perpendicular) turbulent energy cascade rate seems to be sufficient to heat protons in order to explain the Helios observations in the fast solar wind as well. This result, however, may be violated in the high cross-helicity flows often observed in the fast solar wind, where the energy cascade rates estimated from the stationary Kolmogorov-Yaglom law may even become negative [*Smith et al*., 2009], which is problematic.

[43] At 1 AU, the turbulent cascade seems to be able to explain the average proton thermal energetics. To date, there are no estimates of the radial evolution of the turbulent energy cascade based on the Kolmogorov-Yaglom law; there are estimates from the Ulysses spacecraft by *Sorriso-Valvo et al*. [2007] of the radial part of cascade rate in the polar fast solar wind between 3 and 4 AU of the order of 10^2W/kg. This value is much lower than what is observed at 1 AU, which may be connected with the indications that the cascade rate is strongly anisotropic with much weaker cascade in the parallel direction (with respect to the magnetic field), which is expected to be close to the radial direction.

[44] However, the results based on the stationary Kolmogorov-Yaglom law may be questionable in the expanding solar wind. In the expanding solar wind, the Kolmogorov-Yaglom law may be quite generally written as

$$\frac{\partial\left\langle|\delta\boldsymbol{z}^{\pm}|^2\right\rangle}{\partial t} + \nabla_{\delta\boldsymbol{x}}\cdot\langle\delta\boldsymbol{z}^{\mp}|\delta\boldsymbol{z}^{\pm}|^2\rangle = -4\varepsilon_t^{\pm} + \left(\frac{\partial\left\langle|\delta\boldsymbol{z}^{\pm}|^2\right\rangle}{\partial t}\right)_E \tag{17}$$

where the expansion introduces an external forcing term $(\partial\langle|\delta\boldsymbol{z}^{\pm}|^2\rangle/\partial t)_E$. This external forcing has the following form in the approximation of the expanding box:

$$\left(\frac{\partial\left\langle|\delta z^{\pm}|^2\right\rangle}{\partial t}\right)_E = -\frac{v_{sw}}{R}\left\langle|\delta z^{\pm}|^2 + \delta z^{+}\cdot\delta z^{-} - 2\delta z_R^{+}\delta z_R^{-}\right\rangle \tag{18}$$

where we have assumed a small dissipation limit (see Appendix A). The first term on the right-hand side (RHS) of equation (18) gives the WKB evolution, whereas the two other terms give a coupling between $\boldsymbol{z}^{+}$ and $\boldsymbol{z}^{-}$ (i.e., reflection caused by the global solar wind inhomogeneity).

Note that an external forcing similar to equation (18) appears also in a case of velocity shears [*Wan et al*., 2009], which likely play an important role in the solar wind turbulence [*Matthaeus et al*., 1999; *Landi et al*., 2006].

[45] The external forcing due to the expansion (as well as the equivalent forcing due to the velocity shear) appears generally on all scales, which makes the assumption of the stationarity of the turbulence questionable. The estimates based on the stationary Kolmogorov-Yaglom law need to be revisited; it is possible that the negative energy cascade rates obtained from the stationary Kolmogorov-Yaglom law [*Smith et al*., 2009] are a consequence of the stationarity approximation; the external forcing due to the expansion (or a velocity shear) may importantly modify the dissipation rates. Further work is clearly needed to understand the energy cascade rate in the expanding solar wind. The cascading energy repartition on different species and different directions (parallel and perpendicular with respect to the ambient magnetic field) due to the energy cascade of the MHD turbulence are largely unknown. In particular, it is not clear whether the turbulent cascade may be responsible for the parallel cooling observed in the Helios data.

3.7. Kinetic Parallel Cooling

[46] A part of the parallel cooling is connected with the deceleration of the beam with respect to the core (see section 3.5). The relative beam-core velocity seems to follow the local Alfvén velocity, while for nearly radial magnetic field expected around 0.3 AU, this velocity is expected to be about constant. The beam-core structure of the proton velocity distribution function with relative drift velocity of the order of the local Alfvén velocity is likely to be unstable to kinetic instabilities which would constrain the drift velocity around the marginal stability, i.e., around the local Alfvén velocity, which would explain these observations. Linear analysis of the Helios proton observations indeed indicates a presence of kinetic instabilities [*Livi and Marsch*, 1986]. The theoretical expectations based on linear and quasilinear predictions are supported by kinetic simulations [*Hellinger and Trávníček*, 2011], which show that the nonlinear evolution of the beam-core structure in the expanding solar wind keep the beam-core relative velocity around the local Alfvén velocity. It is therefore interesting to compare the simulation results of *Hellinger and Trávníček* [2011] with the Helios observations. The simulation uses the hybrid expanding box approximation, which self-consistently resolves the interaction between the solar wind expansion and ion kinetic effects. The hybrid expanding box simulation exhibits a complicated evolution with different kinetic instabilities, which strongly modify the proton velocity distribution function. This evolution leads to an efficient proton parallel cooling and perpendicular heating in qualitative agreement with the Helios observation in the fast solar wind as well as in the slow solar wind. Here we attempt to compare the simulation results with the Helios observations on a quantitative level. Figure 11 displays the simulated results in a form similar to Figure 5. Figure 11 shows the parallel heating rate $Q_\parallel$ (top panel), the perpendicular heating rate $Q_\perp$ (middle panel), and the average heating rate Q (bottom panel) normalized to the heating rate $Q_E = nk_BT/t_E$ as functions of time. The heating rates in the hybrid expanding box simulation were calculated as the difference between the actual temporal change of the spatially averaged temperatures and the double adiabatic (CGL) prediction [cf., *Matteini et al*., 2012]

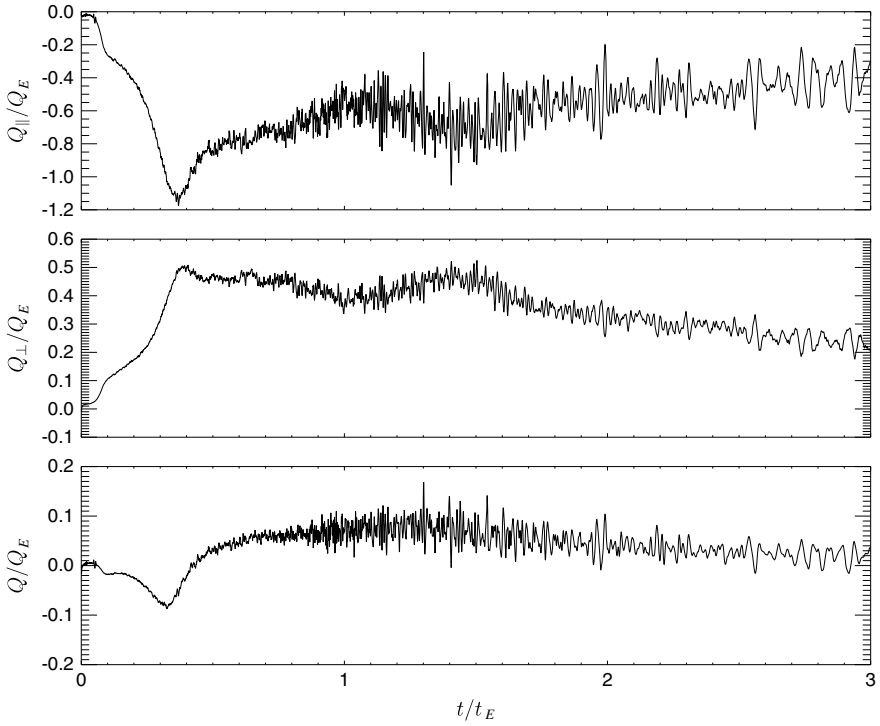

Figure 11. Estimated heating rates from the hybrid expanding box simulation of *Hellinger and Trávníček* [2011]: (top) the parallel heating rate $Q_\parallel$, (middle) the perpendicular heating rate $Q_\perp$, and (bottom) the average heating rate Q normalized to the heating rate Q_E as functions of time.

$$Q_\parallel = nk_B\left[\frac{dT_\parallel}{dt} - \left(\frac{dT_\parallel}{dt}\right)_{CGL}\right]$$
$$Q_\perp = nk_B\left[\frac{dT_\perp}{dt} - \left(\frac{dT_\perp}{dt}\right)_{CGL}\right]. \quad (19)$$

[47] Initially, the heating/cooling rates are negligible. Later on, kinetic instabilities due to the differential core-beam velocity appear, causing parallel cooling and perpendicular heating as well as total cooling as part of the proton energy being transferred to waves. After the saturation, the total cooling decelerate, and there are even indications of a weak total proton heating as some of the generated wave energy is reabsorbed by protons.

[48] The simulation model of *Hellinger and Trávníček* [2011] does not fully describe the complex properties of the solar wind. In particular, it does not include the turbulence/wave activity present in the solar wind, which may influence linear and nonlinear properties of kinetic instabilities [cf., *Nariyuki et al*., 2012]. The simulation model, however, self-consistently resolves the competition between the expansion and kinetic instabilities, and its results indicate that kinetic instabilities generated by the proton beam-core system are capable to cause a parallel cooling of the order of the heating rate Q_E in agreement with Helios observations. Finally, we note that the kinetic mechanism connected with the core-beam structure works for nearly radial magnetic fields, where the expansion tends to increase the relative beam-core velocity with respect to the local Alfvén velocity, and this may explain why the parallel cooling is observed closer to the sun.

4. Conclusion

[49] In this paper, we extended the work of Paper 1 to the slow solar wind. The Helios 1 and 2 observations indicate an increase in the minimum stream velocities with the radial distance This is compatible with an overall acceleration of slow streams as a possible consequence of the interaction between slow and fast streams in agreement with the observations of Paper 1.

[50] We have fitted the radial profiles of proton temperatures. Overall, we find less steep radial gradients than what was obtained by *Marsch et al*. [1982b], but within error bars, we have comparable results. The slow solar wind is typically much more variable than the fast solar wind; here we show that there is a large variability of the proton heat fluxes and the local collisionality. We also show that the local collisionality is not a good proxy to the collisional age, as it remains about constant with the radial distance.

[51] We have estimated the parallel and perpendicular heating rates in the slow solar wind assuming a constant radial velocity. We observe a behavior similar to that observed in the fast solar wind: around 0.3 AU protons need to be cooled in the parallel direction, and further away, there is a need to heat in the parallel direction. Protons need to be heated in the perpendicular direction from 0.3 to 1 AU, and the parallel and perpendicular heating (cooling) rates are comparable. In average, protons need to be heated from 0.3 to 1 AU.

[52] The heating/cooling rates in the fast and slow solar wind are of the same order (in terms of heating per unit volume), and they are naturally expressed in units of the expansion rate Q_E (a ratio between the proton kinetic energy and the expansion time $Q_E = nk_BT/t_E$). The parallel and perpendicular heating/cooling rates constitute typically an important fraction of Q_E, varying about linearly with the distance, whereas the average heating rate remains about constant with the distance.

[53] At 1 AU, the total proton heating rates are below (but constitute an important fraction of) the cascade rates of the MHD turbulence estimated from the stationary Kolmogorov-Yaglom law in the slow and fast solar winds. The assumed stationarity for the Kolmogorov-Yaglom law is, however, questionable in the solar wind.

[54] It is not clear whether MHD turbulence may explain the parallel cooling around 0.3 AU. The cooling is likely a consequence of kinetic instabilities driven by the microstructure (beam-core system) of the proton velocity distribution functions. The beam-core relative velocity decreases with the distance as the local Alfvén velocity, and this phenomenon contributes to the parallel cooling. Natural candidates for the deceleration of the relative beam-core velocities are kinetic beam-type instabilities, which are typically destabilized around beam-core velocity about the local Alfvén velocity. Linear analysis indicates a presence of such instabilities in the solar wind. Numerical simulations of the beam-core system exhibit a nonlinear evolution in qualitative agreement with observations, deceleration of the beam with respect to the core proton population, keeping this velocity about the Alfvén velocity. Moreover, numerical simulations which take into account the solar wind expansion and proton kinetic instabilities exhibit a parallel cooling comparable to the rate Q_E in quantitative agreement with Helios observations.

Appendix A: Kolmogorov-Yaglom Law in the Expanding Box

[55] Some effects which the expansion has on waves and turbulence in the solar wind may be described using the expanding box model [*Grappin et al*., 1993]. This model assumes a radial expansion and takes a parcel of plasma with sizes much smaller than the global scales so that the plasma may be treated as homogeneous on the local/box scales and the curvature effects may be neglected. In the model, the MHD equations are transformed into the frame comoving with the expanding plasma parcel, which moves with a constant solar wind radial velocity v_{sw}. The radial distance R evolves simply as $R = R_0 + v_{sw}t$, where R_0 is an initial radial distance. In these comoving coordinates, the MHD equations may be written in this form [*Grappin and Velli*, 1996]:

$$\frac{\partial \boldsymbol{u}}{\partial t} + (\boldsymbol{u}\cdot\nabla)\boldsymbol{u} - \frac{(\boldsymbol{B}\cdot\nabla)\boldsymbol{B}}{\mu_0\rho} + \frac{\nabla\cdot\mathbf{P}_{tot}}{\rho} = \nu\Delta\boldsymbol{u} - \frac{v_{sw}}{R}\mathbf{T}\cdot\boldsymbol{u} \quad (A1)$$

$$\frac{\partial \boldsymbol{B}}{\partial t} + (\boldsymbol{u}\cdot\nabla)\boldsymbol{B} - (\boldsymbol{B}\cdot\nabla)\boldsymbol{u} + \boldsymbol{B}(\nabla\cdot\boldsymbol{u}) = \eta\Delta\boldsymbol{B} - \frac{v_{sw}}{R}(2\mathbf{R}+\mathbf{T})\cdot\boldsymbol{B} \quad (A2)$$

where $\mathbf{P}_{tot}$ is the total pressure tensor; ν and η are the viscosity and the magnetic diffusivity, respectively; $\mathbf{R}$ is the projection

tensor to the radial direction (i.e., $\mathbf{R}=\boldsymbol{e}_R\boldsymbol{e}_R, \boldsymbol{e}_R$, being the unit vector in the radial direction); and $\mathbf{T}$ is the projection tensor to the transverse directions (i.e., $\mathbf{T}=\mathbf{1}-\mathbf{R}$, $\mathbf{1}$ being the unit tensor). The last term on the RHS of equations (A1) and (A2) constitutes external forces due to the expansion.

[56] Taking the Elsässer variables $\boldsymbol{z}^{\pm}=\boldsymbol{u}\pm\boldsymbol{B}/\sqrt{\mu_0\rho}$, with $\nu=\eta$ (i.e., taking the magnetic Prantl number equal to 1), and neglecting the compressibility effects and pressure gradients, one gets

$$\frac{\partial \boldsymbol{z}^{\pm}}{\partial t}+(\boldsymbol{z}^{\mp}\cdot\nabla)\boldsymbol{z}^{\pm}=\nu\Delta\boldsymbol{z}^{\pm}-\frac{v_{sw}}{2R}\left[\boldsymbol{z}^{\pm}+(\mathbf{1}-2\mathbf{R})\boldsymbol{z}^{\mp}\right] \tag{A3}$$

Defining $\delta\boldsymbol{z}^{\pm}=\boldsymbol{z}^{\pm}(\boldsymbol{x}+\delta\boldsymbol{x})-\boldsymbol{z}^{\pm}(\boldsymbol{x})$ and following the standard procedure assuming homogeneity and incompressibility [cf. *Politano and Pouquet*, 1998; *Carbone et al*., 2009], one gets

$$\begin{aligned}\frac{\partial\left\langle|\delta\boldsymbol{z}^{\pm}|^2\right\rangle}{\partial t}+\nabla_{\delta\boldsymbol{x}}\cdot\langle\delta\boldsymbol{z}^{\mp}|\delta\boldsymbol{z}^{\pm}|^2\rangle=-4\varepsilon_t^{\pm}+2\nu\Delta_{\delta\boldsymbol{x}}\langle|\delta\boldsymbol{z}^{\pm}|^2\rangle\\-\frac{v_{sw}}{R}\left\langle|\delta\boldsymbol{z}^{\pm}|^2+\delta\boldsymbol{z}^{+}\cdot\delta\boldsymbol{z}^{-}-2\delta\boldsymbol{z}_R^{+}\delta\boldsymbol{z}_R^{-}\right\rangle\end{aligned} \tag{A4}$$

where $\langle\,\rangle$ denotes the averaging and $\varepsilon_t^{\pm}$ is the pseudoenergy cascade rate of the corresponding Elsässer variables $\boldsymbol{z}^{\pm}$. The energy cascade rate is then $\varepsilon_t=\left(\varepsilon_t^{+}+\varepsilon_t^{-}\right)/2$. Neglecting the expansion, assuming stationarity, and taking the small dissipation limit ($\nu\Delta_{\delta\boldsymbol{x}}\langle|\delta\boldsymbol{z}^{\pm}|^2\rangle\to 0$), one recovers

$$\nabla_{\delta\boldsymbol{x}}\cdot<\delta\boldsymbol{z}^{\mp}|\delta\boldsymbol{z}^{\pm}|^2>=-4\varepsilon_t^{\pm}. \tag{A5}$$

Appendix B: Glossary

[57] Here $\boldsymbol{B}$ is the magnetic field, $B=|\boldsymbol{B}|$ being its amplitude; $\boldsymbol{b}$ is the unit vector along the magnetic field, $\boldsymbol{b}=\boldsymbol{B}/B$; R stands for the radial distance from the sun, $R_0=1$ AU; and t stands for the time. Here f denotes the proton velocity distribution function, which is assumed to be gyrotropic. Subscripts $\perp$ and $\parallel$ denote the directions with respect to the ambient magnetic field. n is the proton number density $n=\int f d^3v$, $\rho=mn$ is the proton mass density (m being the proton mass), and u is the mean velocity $\boldsymbol{u}=\int \boldsymbol{v} f d^3v$. Here $\boldsymbol{z}^{\pm}=\boldsymbol{u}\pm\boldsymbol{B}/\sqrt{\mu_0\rho}$ are the Elsässer variables (μ_0 being the vacuum magnetic permeability). The parallel and perpendicular proton temperatures are given as $T_{\parallel}=(m/k_Bn)\int v_{\parallel}^2 f d^3v$ and $T_{\perp}=(m/2k_Bn)\int v_{\perp}^2 f d^3v$, respectively, where $v_{\parallel}=\boldsymbol{b}\cdot(\boldsymbol{v}-\boldsymbol{u})$, $v_{\perp}^2=\left|(\boldsymbol{v}-\boldsymbol{u})\right|^2-v_{\parallel}^2$, and k_{B} is the Boltzmann constant; $T=(2T_{\perp}+T_{\parallel})/3$ is the average proton temperature. The two nonzero components of the heat flux tensor are given as $q_{\parallel}=m\int v_{\parallel}^3 f d^3v$ and $q_{\perp}=(m/2)\int v_{\parallel}v_{\perp}^2 f d^3v$, with $q=(2q_{\perp}+q_{\parallel})/3$ being the average proton heat flux. Here, $Q_{\perp}$ and $Q_{\parallel}$ are the necessary perpendicular and parallel heating rates (per unit volume), with $Q=(2Q_{\perp}+Q_{\parallel})/3$ being the average heating rate (note that the total heating rate is 3/2 times Q). Here v_{sw} is the (radial) solar wind velocity, $t_E=R/v_{sw}$ is the characteristic expansion time, and $Q_E=nk_BT/t_E$ is an expansion rate of the proton kinetic energy. Here ε_h is the (proton) heating rate per unit mass $\varepsilon_h=3Q/n/m/2$, $\varepsilon_t^{\pm}$ is the pseudoenergy cascade rate corresponding to $\boldsymbol{z}^{\pm}$, and $\varepsilon_t=\left(\varepsilon_t^{+}+\varepsilon_t^{-}\right)/2$ is the turbulent energy cascade rate. Here ν_T is the proton isotropization frequency [*Hellinger and Trávníček*, 2009]

$$\nu_T=\frac{e^4 n\ln\Lambda}{30\pi^{3/2}\varepsilon_0^2 m^{1/2}k_{\mathrm{B}}{}^{3/2}T_{\parallel}^{3/2}}\,{}_2F_1\left(\begin{matrix}2,3/2\\7/2\end{matrix};1-\frac{T_{\perp}}{T_{\parallel}}\right) \tag{B1}$$

where ε_0 is the permittivity of vacuum and ${}_2F_1$ is the standard Gauss hypergeometric function. Here $\tau=\nu_T t_E$ is the local collisionality factor.

[58] **Acknowledgments.** PH, ŠŠ, and PMT acknowledge grants P209/12/2023 and P209/12/2041 of the Grant Agency of the Czech Republic. The research leading to these results has received funding from the European Commission's Seventh Framework Programme (FP7) under the grant agreement SHOCK (project number 284515, project-shock.eu) and SWIFF (project number 263340, www.swiff.eu). This work was also supported by the projects RVO:67985815 and RVO:68378289.

References

Araneda, J. A., E. Marsch, and A. F. Viñas (2008), Proton core heating and beam formation via parametrically unstable Alfvén-cyclotron waves, *Phys. Rev. Lett.*, *100*, 125003, doi:10.1103/PhysRevLett.100.125003.

Arya, S., and J. W. Freeman (1991), Estimates of solar wind velocity gradients between 0.3 and 1 AU based on velocity probability distributions from HELIOS 1 at perihelion and aphelion, *J. Geophys. Res.*, *96*, 14,183–14,187.

Borovsky, J. E. (2010), On the variations of the solar wind magnetic field about the Parker spiral direction, *J. Geophys. Res.*, *115*, A09101, doi:10.1029/2009JA015040.

Carbone, V. (2012), Scalings, cascade and intermittency in solar wind turbulence, *Space Sci. Rev.*, *172*, 343–360, doi:10.1007/s11214-012-9907-z.

Carbone, V., V. Sorriso-Valvo, and R. Marino (2009), On the turbulent energy cascade in anisotropic magnetohydrodynamic turbulence, *Europhys. Lett.*, *88*, 25001, doi:10.1209/0295-5075/88/25001.

Chew, G. F., M. L. Goldberger, and F. E. Low (1956), The Boltzmann equation and the one fluid hydromagnetic equations in the absence of particle collisions, *Proc. R. Soc. London*, *A236*, 112–118.

Daughton, W., and S. P. Gary (1998), Electromagnetic proton/proton instabilities in the solar wind, *J. Geophys. Res.*, *103*, 20,613–20,620.

Elliott, H. A., C. J. Henney, D. J. McComas, C. W. Smith, and B. J. Vasquez (2012), Temporal and radial variation of the solar wind temperature-speed relationship, *J. Geophys. Res.*, *117*, A09102, doi:10.1029/2011JA017125.

Goldstein, B. E., M. Neugebauer, L. D. Zhang, and S. P. Gary (2000), Observed constraint on proton-proton relative velocities in the solar wind, *Geophys. Res. Lett.*, *27*, 53–56.

Goldstein, B. E., M. Neugebauer, and X.-Y. Zhou (2010), Ulysses observations of the properties of multiple ion beams in the solar wind, in Proceedings of Twelfth International Solar Wind Conference, vol. *1216*, edited by M. Maksimovic, K. Issautier, N. Meyer-Vernet, M. Moncuquet, and F. Pantellini, pp. 261–264, AIP, Melville, New York.

Grappin, R., and M. Velli (1996), Waves and streams in the expanding solar wind, *J. Geophys. Res.*, *101*, 425–444.

Grappin, R., M. Velli, and A. Mangeney (1993), Nonlinear-wave evolution in the expanding solar wind, *Phys. Rev. Lett.*, *70*, 2190–2193.

Hellinger, P., and P. M. Trávníček (2009), On Coulomb collisions in bi-Maxwellian plasmas, *Phys. Plasmas*, *16*, 054501.

Hellinger, P., and P. M. Trávníček (2011), Proton core-beam system in the expanding solar wind: Hybrid simulations, *J. Geophys. Res.*, *116*, A11101, doi:10.1029/2011JA016940.

Hellinger, P., M. Velli, P. Trávníček, S. P. Gary, B. E. Goldstein, and P. C. Liewer (2005), Alfvén wave heating of heavy ions in the expanding solar wind: Hybrid simulations, *J. Geophys. Res.*, *110*, A12109, doi:10.1029/2005JA011244.

Hellinger, P., P. Trávníček, J. C. Kasper, and A. J. Lazarus (2006), Solar wind proton temperature anisotropy: Linear theory and WIND/SWE observations, *Geophys. Res. Lett.*, *33*, L09101, doi:10.1029/2006GL025925.

Hellinger, P., L. Matteini, Š. Štverák, P. M. Trávníček, and E. Marsch (2011), Heating and cooling of protons in the fast solar wind between 0.3 and 1 AU: Helios revisited, *J. Geophys. Res.*, *116*, A09105, doi:10.1029/2011JA016674.

Hollweg, J. V., and P. A. Isenberg (2002), Generation of the fast solar wind: A review with emphasis on the resonant cyclotron interaction, *J. Geophys. Res.*, *107*, 1147, doi:10.1029/2001JA000270.

Kasper, J. C., A. J. Lazarus, and S. P. Gary (2008), Hot solar-wind helium: Direct evidence for local heating by Alfvén-cyclotron dissipation, *Phys. Rev. Lett.*, *101*, 261103.

Landi, S., P. Hellinger, and M. Velli (2006), Heliospheric magnetic field polarity inversion driven by velocity field fluctuations, *Geophys. Res. Lett.*, *32*, L14101, doi:10.1029/2005GL022849.

Li, X., Q. Lu, Y. Chen, B. Li, and L. Xia (2010), A kinetic Alfvén wave and the proton distribution function in the fast solar wind, *Astrophys. J. Lett.*, *719*, L190–L193, doi:10.1088/2041-8205/719/2/L190.

Livi, S., and E. Marsch (1986), On the collisional relaxation of solar wind velocity distributions, *Ann. Geophys.*, *4*, 333–340.

MacBride, B. T., C. W. Smith, and M. A. Forman (2008), The turbulent cascade at 1 AU: Energy transfer and the third-order scaling for MHD, *Astrophys. J.*, *679*, 1644–1660.

Marsch, E. (2012), Helios: Evolution of distribution functions 0.3–1 AU, *Space Sci. Rev.*, *172*, 23–39, doi:10.1007/s11214-010-9734-z.

Marsch, E., and S. Livi (1987), Observational evidence for marginal stability of solar wind ion beams, *J. Geophys. Res.*, *92*, 7263–7268.

Marsch, E., and A. K. Richter (1987), On the equation of state and collision time for a multicomponent, anisotropic solar wind, *Ann. Geophys.*, *5A*, 71–82.

Marsch, E., K. H. Muhlhauser, H. Rosenbauer, R. Schwenn, and F. M. Neubauer (1982a), Solar wind helium ions: Observations of the Helios solar probes between 0.3 AU and 1 AU, *J. Geophys. Res.*, *87*, 35–51.

Marsch, E., K. H. Muhlhauser, R. Schwenn, H. Rosenbauer, W. Pilipp, and F. M. Neubauer (1982b), Solar wind protons: Three-dimensional velocity distributions and derived plasma parameters measured between 0.3 AU and 1 AU, *J. Geophys. Res.*, *87*, 52–72.

Matteini, L., S. Landi, M. Velli, and P. Hellinger (2010), Kinetics of the parametric instabilities of Alfvén waves: evolution of ion distribution functions, *J. Geophys. Res.*, *115*, A09106, doi:10.1029/2009JA014987.

Matteini, L., P. Hellinger, S. Landi, P. M. Travnicek, and M. Velli (2012), Ion kinetics in the solar wind: coupling global expansion to local microphysics, *Space Sci. Rev.*, *172*, 373–396, doi:10.1007/s11214-011-9774-z.

Matteini, L., P. Hellinger, B. E. Goldstein, S. Landi, M. Velli, and M. Neugebauer (2013), Signatures of kinetic instabilities in the solar wind, *J. Geophys. Res.*, *118*, ?, doi:10.1029/2012JA018592.

Matthaeus, W. H., and M. Velli (2011), Who needs turbulence? A review of turbulence effects in the heliosphere and on the fundamental process of reconnection, *Space Sci. Rev.*, *160*, 145–168, doi:10.1007/s11214-011-9793-9.

Matthaeus, W. H., G. P. Zank, C. W. Smith, and S. Oughton (1999), Turbulence, spatial transport, and heating of the solar wind, *Phys. Rev. Lett.*, *82*, 3444–3447.

Miyake, W., T. Mukai, T. Terasawa, and K. Hirao (1988), Stream interaction as a heat source in the solar wind, *Solar Phys.*, *117*, 171–178.

Nariyuki, Y., T. Hada, and K. Tsubouchi (2012), Nonlinear dissipation of circularly polarized Alfvén waves due to the beam-induced obliquely propagating waves, *Phys. Plasmas*, *19*, 082317, doi:10.1063/1.4748296.

Osman, K. T., M. Wan, W. H. Matthaeus, J. M. Weygand, and S. Dasso (2011), Anisotropic third-moment estimates of the energy cascade in solar wind turbulence using multispacecraft data, *Phys. Rev. Lett.*, *107*, 165001, doi:10.1103/PhysRevLett.107.165001.

Osman, K. T., W. H. Matthaeus, M. Wan, and A. F. Rappazzo (2012), Intermittency and local heating in the solar wind, *Phys. Rev. Lett.*, *108*, 261102, doi:10.1103/PhysRevLett.108.261102.

Osmane, A., A. M. Hamza, and K. Meziane (2010), On the generation of proton beams in fast solar wind in the presence of obliquely propagating Alfvén waves, *J. Geophys. Res.*, *115*, A05101, doi:10.1029/2009JA014655.

Politano, H., and A. Pouquet (1998), von Kármán-Howarth equation for magnetohydrodynamics and its consequences on third-order longitudinal structure and correlation functions, *Phys. Rev. E*, *57*, R21–R24.

Schwartz, S. J., W. C. Feldman, and S. P. Gary (1981), The source of proton anisotropy in the high-speed solar wind, *J. Geophys. Res.*, *86*, 541–546.

Smith, C. W., J. E. Stawarz, B. J. Vasquez, M. A. Forman, and B. T. MacBride (2009), Turbulent cascade at 1 AU in high cross-helicity flows, *Phys. Rev. Lett.*, *103*, 201101, doi:10.1103/PhysRevLett.103.201101.

Sorriso-Valvo, L., R. Marino, V. Carbone, A. Noullez, F. Lepreti, P. Veltri, R. Bruno, B. Bavassano, and E. Pietropaolo (2007), Observation of inertial energy cascade in interplanetary space plasma, *Phys. Rev. Lett.*, *99*, 115001.

Tu, C.-Y., and E. Marsch (2001), On cyclotron wave heating and acceleration of solar wind ions in the outer corona, *J. Geophys. Res.*, *106*, 8233–8252.

Tu, C.-Y., E. Marsch, and Z.-R. Qin (2004), Dependence of the proton beam drift velocity on the proton core plasma beta in the solar wind, *J. Geophys. Res.*, *109*, A05101, doi:10.1029/2004JA010391.

Valentini, F., D. Perrone, and P. Veltri (2011), Short-wavelength electrostatic fluctuations in the solar wind, *Astrophys. J.*, *739*, 54, doi:10.1088/0004-637X/739/1/54.

Vasquez, B. J., C. W. Smith, K. Hamilton, B. T. MacBride, and R. J. Leamon (2007), Evaluation of the turbulent energy cascade rates from the upper inertial range in the solar wind at 1 AU, *J. Geophys. Res.*, *112*, A07101, doi:10.1029/2007JA012305.

Verma, M. K., D. A. Roberts, and M. L. Goldstein (1995), Turbulent heating and temperature evolution in the solar wind plasma, *J. Geophys. Res.*, *100*, 19,839–19,850.

Wan, M., S. Servidio, S. Oughton, and W. H. Matthaeus (2009), The third-order law for increments in magnetohydrodynamic turbulence with constant shear, *Phys. Plasmas*, *16*, 090703, doi:10.1063/1.3240333.